Electrochimica Acta 322 (2019) 134752

Contents lists available at ScienceDirect

Electrochimica Acta

journal homepage: www.elsevier.com/locate/electacta

In-situ monitoring of hydrogen absorption into Ni thin film electrodes during alkaline water electrolysis

Joris Proost*, Adeline Delvaux

Institute of Mechanics, Materials and Civil Engineering, Université Catholique de Louvain, B-1348, Louvain-la-Neuve, Belgium

ARTICLE INFO

Article history:
Received 14 April 2019
Received in revised form
30 July 2019
Accepted 21 August 2019
Available online 21 August 2019

Keywords:
Hydrogen evolution
Water electrolysis
Absorption
Hydriding
Nickel

ABSTRACT

Although hydrogen production by water electrolysis has already been studied intensively, research efforts continue to be directed towards further improving the electrochemical kinetics and the overall cell efficiency. The objective of the current work is to address an often overlooked parasitic reaction step during the hydrogen evolution reaction (HER), namely the diffusion and absorption of hydrogen adatoms from the electrode surface into the bulk. Chrono-amperometric measurements have been realised in a homemade electrochemical cell on Ni thin film samples. The latter were coupled to a multi-beam optical sensor to obtain high resolution in-situ curvature measurements during the HER. In the thin film geometry, hydrogen absorption into the electrode results in a constrained volume expansion. This in turn leads to internal stress generation, which can be monitored in-situ by means of curvature measurements. Our results on Ni thin film electrodes during alkaline water electrolysis show that such in-situ curvature measurements allow to study both the kinetics and the amount of hydrogen absorption in great detail. In particular, we observed that a higher fraction of hydrogen is being absorbed into the electrode at low overpotential, and that the rate of absorption increases significantly with increasing overpotential. We also discuss the impact of these observations on the identification of the rate-determining steps during a typical HER polarisation curve.

1. Introduction

With the increasing energy demand and the resulting risk of global warming, conventional polluting hydrocarbon fuels need to be replaced by greener ones. In this context, hydrogen from water electrolysis seems to be a promising candidate as carbon-neutral energy carrier [1]. Water electrolysis has been intensively looked at over the last decade, because of its stable output, the availability of simple reactants and a high H_2 purity [2,3]. From an electrochemical perspective, an important aspect of hydrogen production by water electrolysis is the binding energy between the metallic electrode and hydrogen atoms adsorbed on its surface after water (or proton) reduction. If this binding energy is too strong, hydrogen adatoms will not desorb and are not able to recombine into dihydrogen gas. On the other hand, if the bond is too weak, the atoms are not adsorbed on the electrode and the reaction does not occur [4]. For a constant hydrogen evolution reaction (HER) rate at the electrode surface, it is well understood that depending on the rate-limiting step, the required overpotential will decrease when the energetics of adsorption of reaction intermediates on the electrode surface is more favourable. As a result, a better understanding of the hydrogen ad- and absorption mechanisms on the electrode surface is of utmost importance.

The objective of the current paper is to present and validate a new method to study the absorption of hydrogen into the electrode in real time during HER. It is based on a high-resolution in-situ curvature measurement technique, using a multi-beam optical sensor (MOS) which records the distance variations between an array of parallel laser beams reflecting off the electrode backside. Thin films of nickel were used as the electrode material of choice, since Ni is the primary candidate material for the HER in alkaline conditions due to its low cost, relative abundance, its high electrochemical activity and its long-term stability [5,6]. In the thin film geometry, hydrogen absorption into the electrode leads to a constrained volume expansion, since the thin film electrode is attached to an inert substrate. This then results in internal stresses inside the film, and therefore in a sample curvature. This paper demonstrates how such in-situ curvature measurements allow to address both the kinetics and the amount of hydrogen absorption in great detail.

* Corresponding author.
E-mail address: joris.proost@uclouvain.be (J. Proost).

https://doi.org/10.1016/j.electacta.2019.134752
0013-4686/

2. Experimental

2.1. Electrode preparation

Ni thin films were deposited by magnetron sputtering from a pure Ni target (K.J. Lester Co.) onto a double-sided polished, 380 μm thick silicon substrate. The deposition power and time in our multi-target sputtering chamber (Orion 5 from AJA I'nal) were set at 40 W and 75 min, respectively, aiming for a Ni thin film thickness of about 100 nm. For the 2 replica films that have been deposited, the exact thickness was determined by Inductively Coupled Plasma – Optical Emission Spectrometry (Agilent Technologies 5100 ICP-OES) after complete dissolution of the Ni layer in a 50-50 $\%_{wt}$ $HCl-HNO_3$ acid solution. The chemical detection limit for Ni was on the order of 0.01 ppm, resulting in a thickness resolution of 0.1 nm. The ICP-OES technique was also used to determine the purity of the films: no contaminants in concentrations higher than 10 ppm have been detected.

Before the Ni deposition process, the Si substrate was cleaned in a H_2SO_4/H_2O_2 bath (5:2 in volume) at 80 °C during 10 min, dipped in 2% HF during 20 s to etch away its native oxide, and rinsed in ultra-pure H_2O during 10 min. Immediately after cleaning, the Si substrate was loaded into the sputtering chamber and passivated with a 4 nm TiO_2 layer by RF sputtering from a TiO_2 target. This oxide layer is mainly used as an adhesion layer for the following Ni deposition, since the film tends to delaminate when in contact with the KOH solution. It also helps to prevent any oxidation of the Si (SiO_2 being fully insulating), while still allowing facile electron transfer between the Si substrate and the overlying Ni catalyst. Indeed, its tunnelling properties are well-documented in the literature over a relatively wide thickness range of 0.5–7 nm [7].

The Ni films were then deposited onto the TiO_2 layer without breaking the vacuum. The base pressure prior to TiO_2 and Ni depositions was 1.10^{-7} Torr, while sputtering itself was performed in an Ar atmosphere at 2 and 5 mTorr for TiO_2 and Ni, respectively. Purity levels of the TiO_2 and Ni targets were respectively 99.99% and 99.995. Based on a series of detailed cross-sectional TEM micrographs with automated crystallographic orientation mapping (ACOM), our Ni thin films were shown to be crystalline, exhibiting a dominant (101) texture along the film thickness, with an average grain size of 20 nm and a Σ3 twin boundary density of 14 $\mu m/\mu m^2$.

Since the electrodes are always stored for a few days before being used, a native Ni oxide will be formed on the electrode surface, which could potentially be a resistance barrier for hydrogen incorporation. In the case of a Ni (111) single crystal for instance, an air-formed oxide with a thickness of about 0.5 nm has been reported due to the dissociative chemisorption of oxygen on Ni [8]. The composition of this native oxide layer has already been extensively investigated in the literature. Some works claim that it is composed of non-stoichiometric NiO_x [9], while others concluded that the air-formed oxide is composed of an α-$Ni(OH)_2$ layer overlying the non-stoichiometric NiO_x [10]. In any case, upon first immersion at open circuit potential into 1.0 M KOH (which is also the electrolyte being used in our case), additional hydroxide is instantaneously formed on top of the air-formed oxide. Its thickness was measured from X-ray reflectivity data to be on the order of 0.9 nm [8]. However, these authors also convincingly showed that both the oxide and hydroxide are reduced back to metallic Ni upon cathodic polarisation before H_2 evolution takes off. These reported observations are also in line with the Pourbaix diagram of Ni, where from pH 9 onwards, the border for entering the Ni stability region starts well before the equilibrium potential for H_2 evolution [11].

2.2. Electrochemical measurements

Our measurement setup is schematically presented in Fig. 1, and has already been described in detail elsewhere [12]. It consists in a home-made, 100 mL PTFE electrochemical cell, in which no glass components have been used in order to avoid any possible contamination resulting from glass etching in alkaline solutions. The cell was also systematically cleaned into ultra-pure water (18.2 MΩ cm) before and after each experiment. KOH pellets (≤0.001% trace metals, Sigma-Aldrich) and ultra-pure water were used to prepare the 1 mol/L KOH electrolyte. The equilibrium potential was set at 0 V vs. the Reversible Hydrogen Electrode (RHE) by purging the electrolyte with 99.999% pure N_2 (Air Liquide) during 30 min, in order to minimize the amount of any residual oxygen. The counter electrode was a Pt mesh ($1.7 \times 3.3\ cm^2$) and the reference electrode a Hg/HgO/KOH 1 mol/L (both from Radiometer Analytical). All potentials reported in this paper are referenced to the RHE:

$$E_{RHE} = E_{Hg/HgO} + E_{T,corr} + 0.059pH \quad (1)$$

with $E_{Hg/HgO}$ the measured potential and $E_{T,corr}$ the temperature correction factor for the Hg/HgO/KOH 1 mol/L reference electrode, equal to 0.129 V at 20 °C. The pH value of the electrolyte that appears in eq. (1) was measured by a standard pH meter to be around 14.4 before each chrono-amperometric experiment. We also performed one single continuous pH measurement at 200 mV cathodic overpotential, i.e. the condition with the highest H_2 evolution rate, and found the pH to increase only slightly (by 0.04) in the course of the experiment.

All electrochemical experiments were performed using a Metrohm Autolab PGSTAT302 N potentiostat, and consisted in chrono-amperometric measurements during 100 s at different cathodic overpotentials (10, 50, 100 and 200 mV). A reference, triple cycled CV-scan was taken as well in the cathodic direction between 0 and 4 V with a scan rate of 10 mV/s. In order to check that the obtained CV data are at equilibrium, additional CV scans at different scan rates have first been performed as well. It was found that increasing the scan rate from 5 up to 200 mV/s leads to a larger hysteresis between the forward and backward scans, especially at low overpotential. The more equilibrated curves are therefore the ones with the lowest hysteresis, i.e. for the lowest scan rates (5 and 10 mV/s).

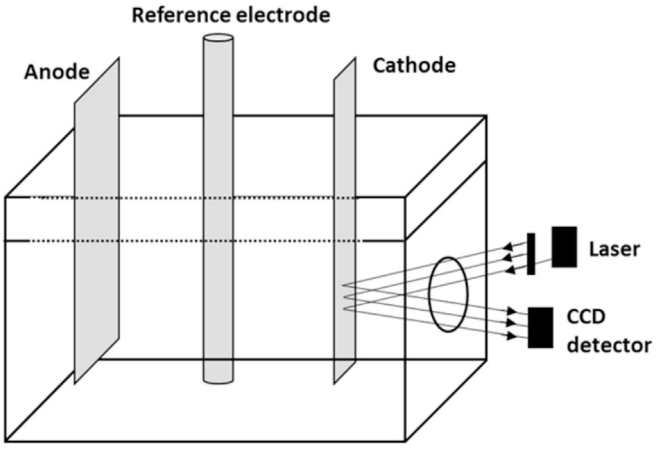

Fig. 1. Schematics of the electrochemical setup, showing the 3 electrodes and the multi-beam optical sensor used for high-resolution in-situ curvature measurements.

As a result, we can expect that the CV realised in our work at 10 mV/s is indeed close to equilibrium. Moreover, as already detailed above, 3 cycles have always been performed. The fact that they almost superposed as well is an additional reliable indication that they are indeed at equilibrium.

2.3. High resolution in-situ curvature measurements

In order to be able to determine the hydrogen uptake from in-situ curvature measurements, the Ni thin film working electrode was mounted vertically as a cantilevered sample, cut approximately $4 \times 0.5\ cm^2$ in size. For a correct current density calculation, the exact area of the electrode that was exposed to the electrolyte was determined after the electrochemical experiments by optically scanning the electrode and analysing its contours with image recognition software (ImageJ). Our high resolution in-situ curvature measurement setup (MOSS, from k-Space) detects in real time the spacings between 4 laser beams deflecting off the backside of the Ni thin film sample with a charge coupled device (CCD) camera. The sample curvature $\Delta\kappa$ is then calculated from the mean value $\frac{\Delta D}{D_0}$ of the differential spacings between these 4 spots:

$$\Delta\kappa = \frac{\cos\alpha}{2L.n}\cdot\frac{\Delta D}{D_0} \tag{2}$$

where $\alpha$is the angle of laser incidence on the sample, L the distance between the sample and the CCD camera, and n the refractive index of the electrolyte (being 1.42 for 1.0 M KOH [13]). By using such multiple beam reflexions, we already showed before [14] that it is possible to significantly reduce the instability of the curvature measurement due to vibrations. In the current configuration, it resulted in an increased dynamic resolution on the radius of curvature of ~10 km, combined with a time resolution better than 100 ms thanks to the use of a CCD camera. Finally, the internal stress change $\Delta\sigma_H$ due to H-absorption into the Ni thin film electrode can be derived from the curvature change $\Delta\kappa$ using the well-known Stoney equation:

$$\Delta\sigma_H = \frac{Y_s.\,t_s^2}{6t_f}\Delta\kappa \tag{3}$$

with $Y_s = E_s/(1-\upsilon_s)$ the biaxial elastic modulus of the substrate (E_s being its Young modulus and υ_s the Poisson ratio), and t_s and t_f the substrate and Ni thin film thickness, respectively.

3. Results and discussion

3.1. Alkaline water electrolysis

First of all, in order to have a general insight in the electrochemical rate-determining step(s) during alkaline water electrolysis on our Ni thin film electrodes, a full CV scan was taken up to a cathodic overpotential of 4 V. The result for the 3rd cycle is shown in Fig. 2, which also includes as an inset the details of all 3 cycles at low overpotential. Apart from the well-expected appearance of a limiting current density at high overpotentials (>2 V), and an upward curvature at low overpotential (<100 mV) that will be discussed later, the overall observed semi-logarithmic behaviour between the current density and the applied potential seems to indicate that the electrochemical kinetics are at least qualitatively in agreement with the well-known Butler-Volmer equation under cathodic conditions [15]:

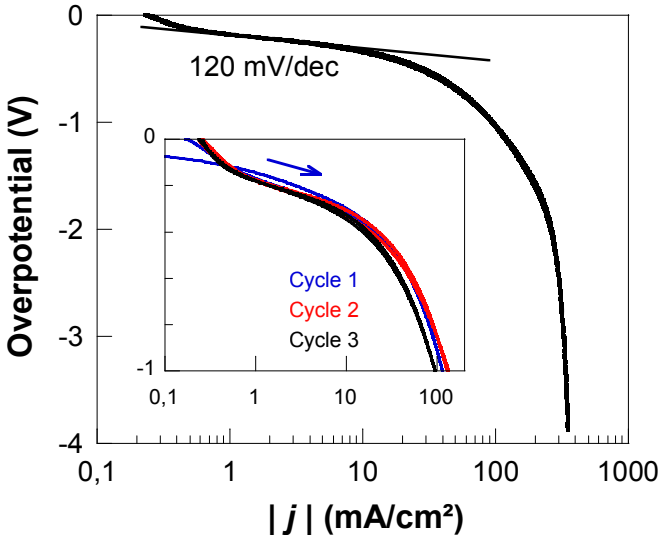

Fig. 2. Tafel plot of a C–V scan of in the cathodic direction up to an overpotential of 4 V (scan rate 10 mV/s). The details of all 3 cycles at low overpotential are shown in the inset.

$$I_c = I_0 * \exp\left(\frac{-\alpha F\eta}{RT}\right) \tag{4}$$

with I_c the cathodic current density, I_o the exchange current density, α the charge transfer coefficient, η the activation overpotential, and R, F and T having their usual meaning. However, when quantitatively comparing the observed C–V plot in Fig. 2 to the simulated Tafel plots for alkaline water electrolysis in Fig. 3 (reproduced from Shinagawa et al. [16]), none of the 3 theoretical cases (each corresponding to a different rate-determining step) correspond to our own experimental result. In the first case (Fig. 3a), the hydrogen evolution reaction is taken to be rate-limited by the initial, one-electron reductive adsorption of hydrogen at the electrode surface, also known as the Volmer reaction:

$$H_2O + e^- = H_{ads} + OH^- \tag{5}$$

In this case, a Tafel slope of 120 mV/dec is observed, as in our case, but no limiting current density is expected. In the second case (Fig. 3b), it is the electrochemical desorption step, known as the Heyrovsky reaction, which is taken to be rate-determining:

$$H_{ads} + H_2O + e^- = H_{2(g)} + OH^- \tag{6}$$

Again, this would result in a Tafel slope of 120 mV/dec over most of the polarisation curve, but no limiting current is expected in this case neither. The latter is mainly due to the saturation of the surface coverage θ of adsorbed H, represented as a dashed curve in Fig. 3 b as well (and clearly demonstrating the often overlooked Tafel slope dependence on surface coverage). The third case (Fig. 3c), in which the desorption process is assumed to consist in the recombination of two adsorbed hydrogen atoms at the electrode surface (Tafel reaction)

$$2\,H_{ads} = H_{2(g)} \tag{7}$$

Looks qualitatively the most similar to our own C–V because of the appearance of a limiting current density. However, a Tafel slope of only 30 mV/dec is expected in this case, accompanying an exponentially increasing surface coverage. The above theoretical

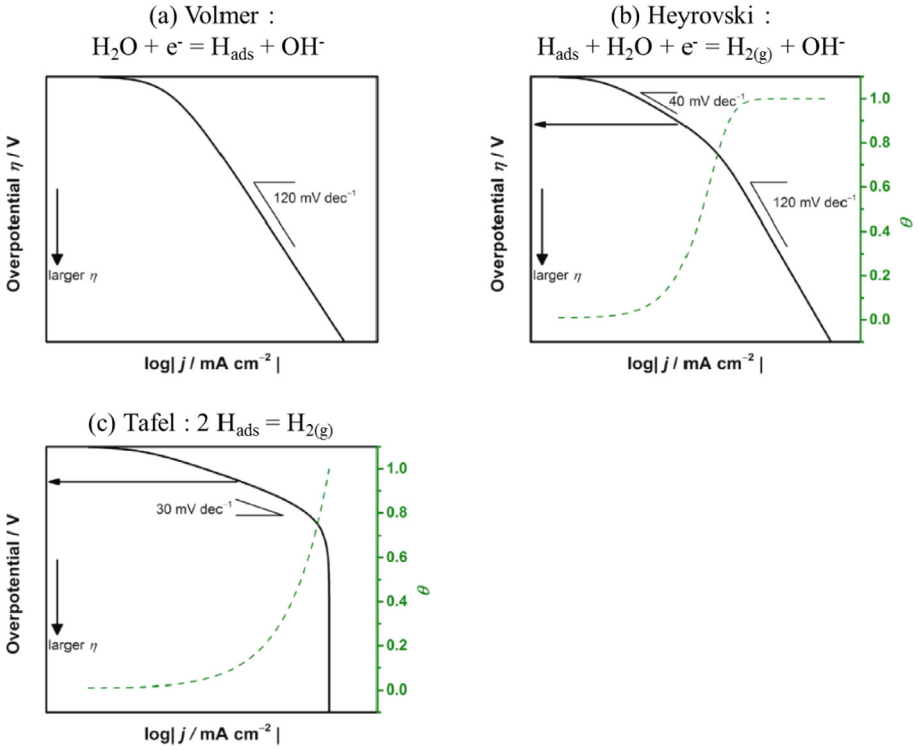

Fig. 3. Simulated Tafel plots for the hydrogen evolution reaction (HER), assuming the (a) Volmer, (b) Heyrovsky and (c) Tafel reaction as the rate-limiting step. Reproduced from Ref. [16].

cases have recently been extended by Vilekar et al. [17] to combinations where 2 or 3 steps are rate-determining. By exploiting the electrical analogy of the alkaline water electrolysis reaction network, they thus obtained separate rate expressions for the Volmer-Tafel, Volmer-Heyrovsky, Heyrovsky-Tafel and Tafel-Volmer-Heyrovsky mechanism, respectively. However, in none of the above a combination of a Tafel slope of 120 mV/dec with the occurrence of a limiting current has been predicted. We believe that this can be attributed to the fact that an important additional reaction pathway has been overlooked so far, namely the parasitic absorption of adsorbed hydrogen species from the surface into the bulk of the electrode:

$$H_{ads} = H_{abs} \quad (8)$$

As illustrated schematically in Fig. 4, this additional reaction will have a direct impact on the available adsorbed hydrogen atoms H_{ads} on the electrode surface, and hence the surface coverage θ, the latter being well-known from Fig. 3 to directly affect the Tafel slope as well.

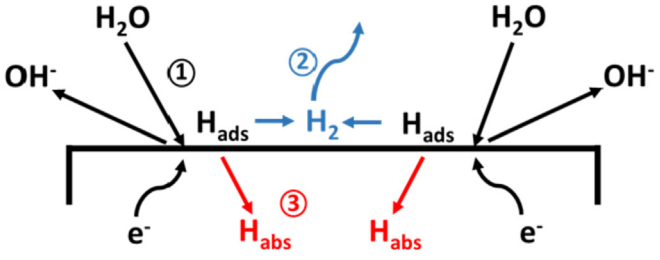

Fig. 4. Schematics of possible rate-determining reactions taking place during HER: (1) Volmer reaction, (2) Tafel reaction and (3) hydrogen absorption into the electrode.

We therefore directed the rest of our study in trying to quantitatively address the effect of hydrogen absorption during alkaline water electrolysis at different, fixed overpotentials. Due to instrumental limitations, these chrono-amperometric measurements had to be limited to relatively small overpotentials, up to 200 mV. Indeed, at higher potentials, the increasing amount of hydrogen bubbles causes flow patterns into the electrolyte, leading in turn to severe perturbations of the laser beams which make the in-situ curvature measurements unreliable. Fig. 5 a shows the time evolution of the current density during such chrono-amperometric experiment for different cathodic overpotentials. In order to be able to compare these measurements at constant overpotential to the results of Fig. 2 obtained during a dynamic C–V scan, Fig. 5 b also shows a superposition of the latter (zoomed up to 400 mV) with both the initial and stabilised current densities during chrono-amperometry. A shift is observed between the 2 data series, due to the simple fact that the initial current densities are maximum, non-equilibrium values at the very beginning of a cathodic step [18]. It is especially re-assuring to observe that the stabilised data approach the CV scan, which we already showed before also to be at equilibrium. In any case, the dependence between current density and overpotential, as quantified by the Tafel slope, is very similar in all cases, so that we can be confident that results from these chrono-amperometic measurements will still be meaningful for understanding to what extent hydrogen absorption affects the electrochemical kinetics at higher overpotentials as well.

3.2. Hydrogen absorption during alkaline water electrolysis

As explained before, our in-situ measurement of hydrogen uptake is based on the fact that hydrogen incorporation into the Ni thin film electrode leads to a constrained volume expansion, generating internal stresses $\Delta\sigma_H$ into the film. We already demonstrated elsewhere how these stresses can be directly related,

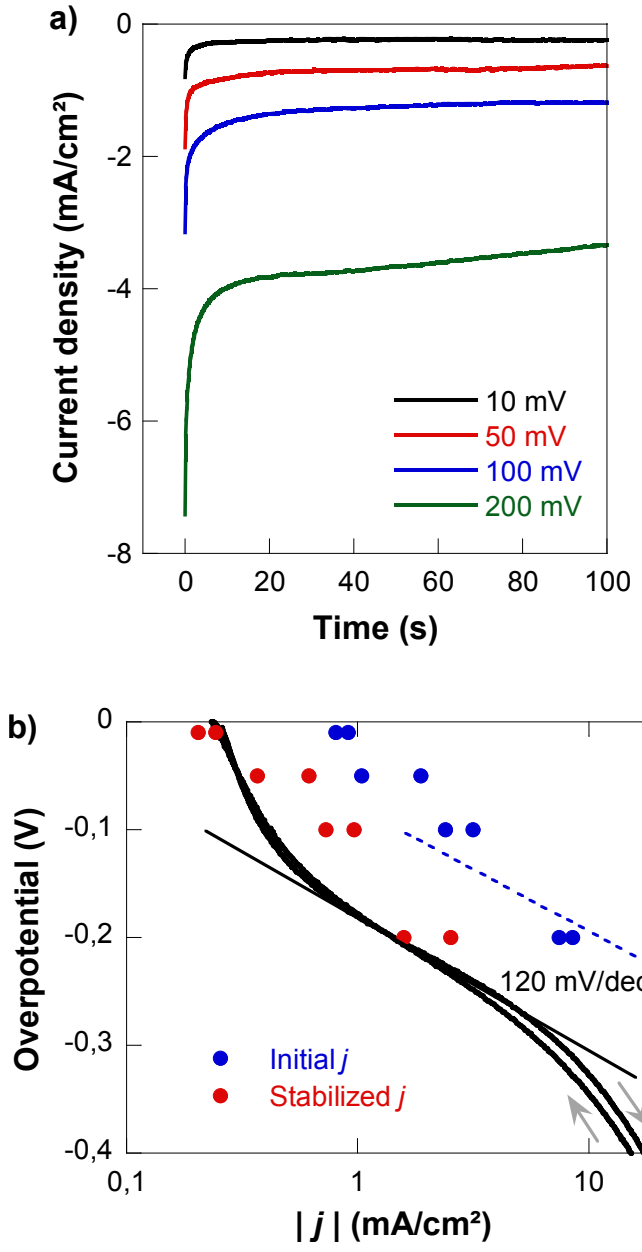

Fig. 5. a) Time evolution of the current density during chrono-amperometric experiments at different cathodic overpotentials, b) Superposition of the initial and stabilised current densities obtained during chrono-amperometry and the C–V scan shown in Fig. 2 (zoomed to 400 mV).

at least in the elastic regime, to the H/Ni atomic ratio $N_{H/Ni}$ [19]:

$$\Delta\sigma_H = \frac{E_f}{3\left(1-\upsilon_f\right)} \cdot \left(\frac{\Delta v}{\Omega_{Ni}}\right) \cdot N_{H/Ni} \tag{10}$$

with E_f and ν_f the Young modulus and Poisson ratio of the Ni film (equal to 205 GPa and 0.31, respectively [20]), Δv the characteristic volume change per hydrogen atom, and Ω_{Ni} the molar volume of Ni. Values for Δv and Ω_{Ni} were taken from Ref. [21] as 2.42 Å^3/atom and 6.6 cm^3/mol, respectively. The absolute amount of hydrogen $n_{H,Ni}$ absorbed into the Ni electrode during HER can then be calculated (in mol/cm^2) as:

$$n_{H,Ni} = N_{H/Ni}.n_{Ni} \tag{11}$$

where n_{Ni} is the number of mol of Ni per cm^2 of thin film, as determined by ICP-OES.

Fig. 6 then represents the evolution of the internal stress change due to hydrogen absorption associated with the chrono-amperometric measurements shown in Fig. 5 a. From a qualitative point of view, one can see that the stress slope becomes steeper, and that the stress curves stabilize quicker when increasing the cathodic overpotential. This is confirmed more quantitatively in Fig. 7, which shows in part (a) both the absolute ($n_{H,Ni}$) and relative ($N_{H/Ni}$) amount of absorbed H corresponding to the maximum stress change, and in part (b) the time corresponding to this maximum. From Fig. 7(a), it appears that the amount of absorbed hydrogen is independent of overpotential, the obtained average H/Ni atomic ratio of 0.011 ± 0.001 being indicative for the presence of α-hydride, i.e. a solid solution of hydrogen atoms in the octahedral interstices of Ni. The latter has indeed been shown to be the stable hydride phase up to a H/Ni ratio of 0.03 [22], while above 0.6 only the β-hydride phase can exist [23]. From the generic Hydrogen-Metal (H/M) phase diagram, a 2-phase matrix of α and β phases can be expected between these two ratio's, as is already well-known for Pd and other metal hydrides [24]. Indeed, when storing gaseous hydrogen in Pd, the hydride consists in an α-phase when H/Pd < 0.02, a β-phase when H/Pd > 0.58 and a mix of α-β between these two ratios' [25]. With respect to the different behaviour of the α and β phases, the Ni β-hydride has the same FCC lattice structure than the α-phase, except that all the octahedral interstices are occupied by hydrogen atoms. Moreover it has a lattice parameter which is 6% larger than that of pure Ni, as compared to only 1% for the α-phase which has only hydrogen atoms in solid solution. Therefore, since only β-hydride is believed to act as a diffusion barrier for continued hydrogen uptake [26], it cannot be held responsible in our case for the limited and fixed

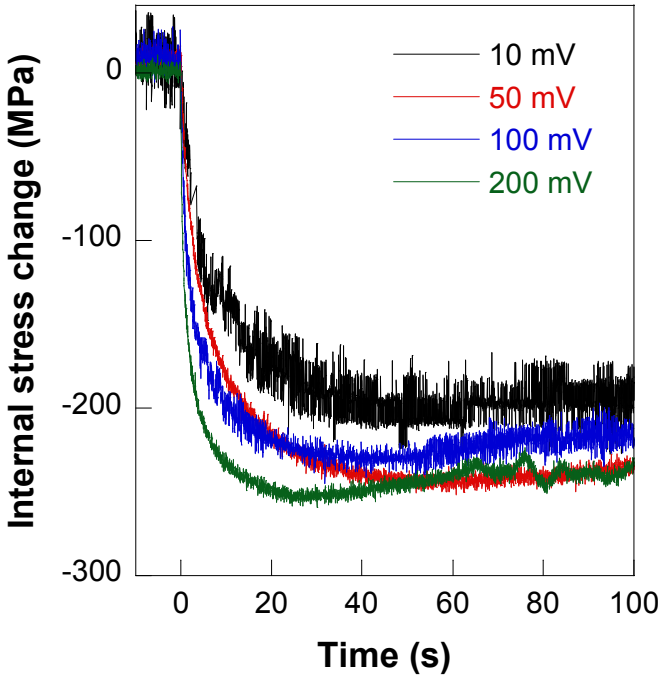

Fig. 6. Time evolution of the internal stress change resulting from hydrogen absorption into the Ni thin film electrode during chrono-amperometric measurements at different cathodic potentials.

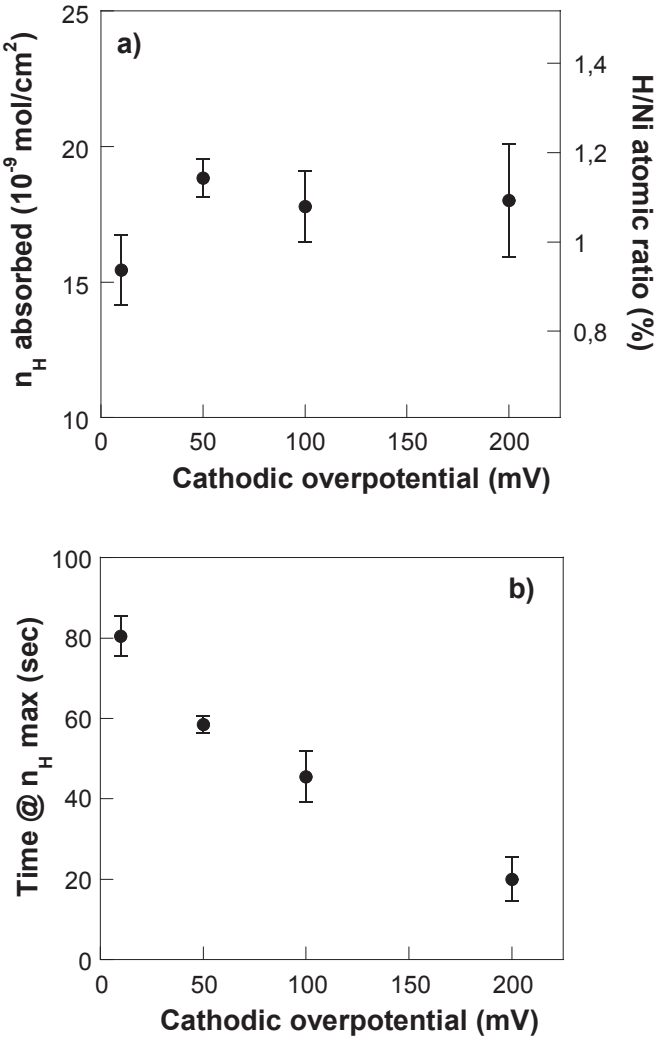

Fig. 7. a) The absolute ($\boldsymbol{n_{H,Ni}}$) and relative ($N_{H/Ni}$) amount of absorbed H as a function of cathodic overpotential, corresponding to the maximum stress change in Fig. 5(b) the time needed before reaching this maximum.

amount of hydrogen absorption in our Ni thin film electrode.

From Fig. 7(b), it then follows that it is only the rate at which this hydrogen is being absorbed that can be affected, resulting in an apparently faster hydrogen saturation of the Ni thin film at higher overpotentials. One plausible explanation for this observation is that fact that a higher overpotential also induces a higher hydrogen evolution current, which according to the Volmer reaction (5) then also generates a higher amount of H_{ads} per unit time. In this respect, Fig. 8 shows the fraction of hydrogen absorbed into the Ni thin film electrode, relative to the theoretical amount of gaseous hydrogen produced from the HER during chrono-amperometry. The latter can be calculated from Faraday's law

$$n_{H,Far} = \frac{J\,t}{F\,z} \tag{12}$$

where z is the number of electrons exchanged, and $n_{H,Far}$ the number of mol of hydrogen per cm^2 theoretically produced during chono-amperometry, obtained by integrating the measured current density shown in Fig. 5 over time. The fraction of absorbed hydrogen in Fig. 8 is then calculated from the ratio between $n_{H,Ni}$ and $n_{H,Far}$, with $n_{H,Ni}$ being taken at the stress maximum. From this

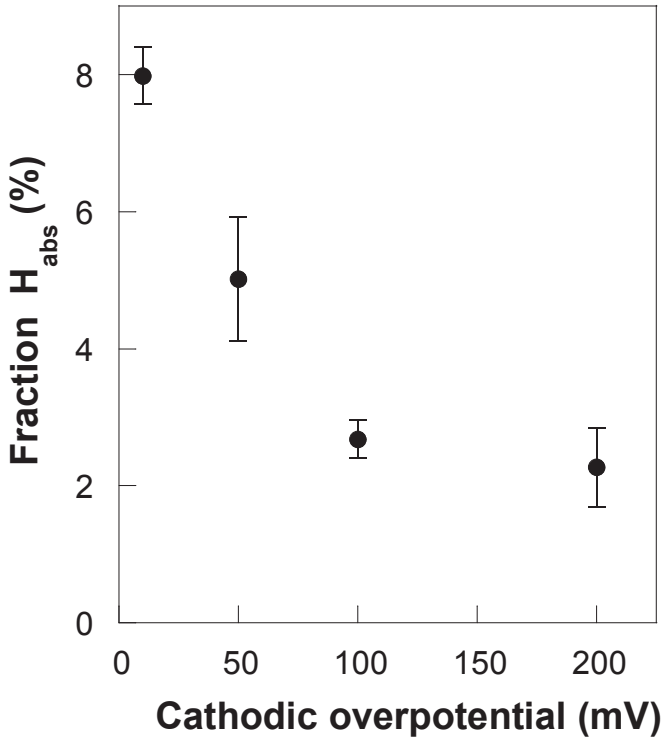

Fig. 8. Atomic percentage of hydrogen absorbed into the nickel thin film electrode in comparison with the hydrogen theoretically produced as a function of the applied potentials.

graph, one can indeed see that a relatively more important fraction of hydrogen is being absorbed into the Ni thin film at lower overpotential. These observations are already indicative for the importance of taking into account hydrogen absorption as well among all possible competing reactions occurring at the electrode surface during hydrogen evolution. Indeed, when the kinetics of the hydrogen evolution is slow, i.e. at low overpotential and hence low current density, the adsorbed hydrogen H_{ads} generated at the electrode surface by the Volmer reaction (11) still has sufficient time to diffuse into the Ni electrode before the Tafel or Heyrovski recombination steps take place. When increasing the potential, the Volmer reaction speeds up, hence generating more H_{ads} per unit time. As a result, the fraction of H_{ads} that will get absorbed also decreases due to the more limited time for H_{ads} to diffuse into the Ni lattice before the recombination step(s) take(s) place.

To complete the kinetic analysis, the hydrogen absorption rates have been calculated as well. To this end, the stress data from Fig. 6 have been fit to an exponentially decreasing time function [19].

$$\Delta\sigma_H = A^*\left[1 - \exp\left(-\frac{t}{B}\right)\right] \tag{13}$$

where B can be interpreted as a time constant for absorption, and A being a characteristic pre-factor which is semi-empirically related to the mechanistic details of the absorption process [19]. For the current work, we limit ourselves to using the fitted values of A and B for quantifying the initial slope of the stress curve at the beginning of the potential step. Indeed, from a simple time derivative of eq. (13), the initial rate of absorption can be taken to be proportional to

$$\left(\frac{d\Delta\sigma}{dt}\right)_{t=0} = -\frac{A}{B} \tag{14}$$

The thus obtained initial hydrogen absorption rates (in MPa/sec)

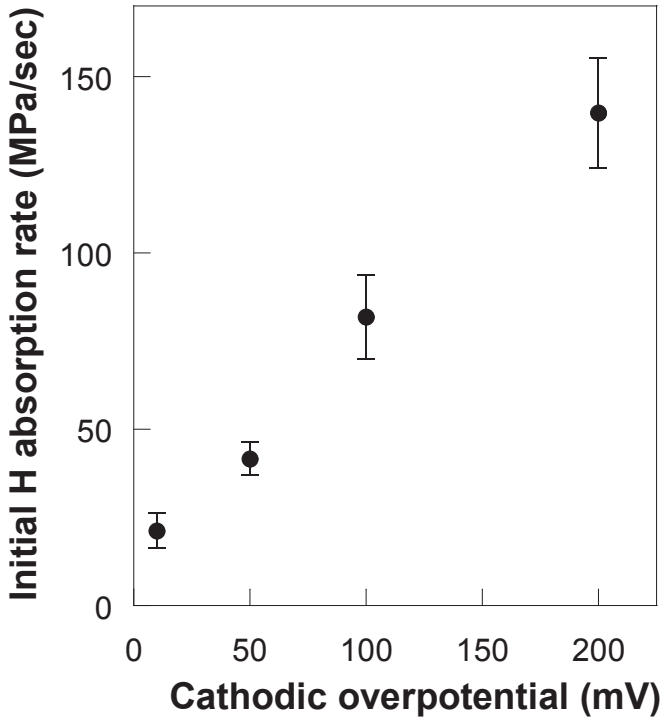

Fig. 9. Initial hydrogen absorption rates (in MPa/sec) as a function of cathodic overpotential, as obtained from the derivative of the stress curves at $t = 0$.

are shown in Fig. 9 as a function of cathodic overpotential. One can see that they increase significantly with potential, by almost a factor 4 between 10 and 100 mV. As a result, at high overpotential (>100 mV), it can be expected that a high recombination rate of adsorbed species according to the Tafel reaction (7) coincides with a very quick absorption of the hydrogen adatoms into the Ni thin film, although in a relatively low amount with respect to the net amount of evolved gaseous H_2. At low overpotential (<100 mV), the hydrogen absorption rate is lower, but also the electrode surface is charged more slowly, resulting in a low recombination rate of adsorbed hydrogen atoms at the electrode surface and a still relatively high amount of H_{ads} being injected into the bulk electrode.

Based on all of the above observations, we can now try to rationalize the particular features of the polarisation curve in Fig. 2 for our Ni thin film electrodes shown in the very beginning. Firstly, with respect to the "upward curvature" at small overpotential (<100 mV), this is clearly the region where absorption of H_{ads} is most pronounced. Graphically, its effect is fully similar to the gradual appearance of a limiting current at the highest overpotential. Such a "limiting current" at low overpotential can be understood as being the result of a lack of reactive species H_{ads}, not because of transport or diffusional limitations, but because these rate-controlling reactive species in that specific overpotential region preferably get absorbed into the bulk electrode (and also have the time to do so). Secondly, upon increasing the cathodic overpotential beyond 100 mV, a Tafel slope of about 120 mV/dec starts to establish. According to Fig. 3, this value is indicative for the Volmer reaction (eq. (5)) to become rate-determining. Since the Heyrovsky reaction is not very likely to occur during alkaline water electrolysis on Ni electrodes [22], the Volmer reactions in our case also the only possible step involving electron transfer. In particular, this step is believed to be rate-controlling rather than the Tafel recombination step (eq. (7)) because of Ni hydride formation at lower overpotential. In this respect, Soares et al. [27] convincingly showed that hydrogen incorporation into a Ni electrode changes the d-character of the metal to a s-p character, hence decreasing the density of states at the Fermi energy level, as well as its electrocatalytic activity. In other words, electron transfer for water reduction into H_{ads} should become more difficult for Ni–H than for pure Ni, making the Volmer reaction indeed rate-controlling once Ni hydride is being formed. Moreover, Kim et al. [28] recently demonstrated that compressive stresses in a Ni thin film electrode also induce a downshift of the d-orbital in comparison to the Fermi level, resulting in a lower Ni–H binding strength. This should make it easier for adsorbed H to recombine at the electrode surface, another argument in favour of the Volmer and not the Tafel reaction being rate-controlling. Thirdly, at still higher overpotential, when electron transfer is no longer rate-limiting, the surface coverage θ of adsorbed H will tend to unity, as in Fig. 3c, and a limiting current will appear.

Finally, we would like to recognise that it is still unclear at the moment to what extend all of the above insights obtained on pure Ni thin film model electrodes can be transferred to the Ni bulk electrodes being used in industrial water electrolysers. Indeed, significant microstructural difference exist between both, not the least in terms of grain size. We are therefore currently trying to address the effect of microstructure on hydrogen absorption by depositing Ni thin films at different sputter conditions.

4. Conclusions

We have reported and validated a new experimental setup that allows to study both the amount and the kinetics of hydrogen absorption into Ni thin film electrodes in real-time during the HER. During a series of well-designed chrono-amperometric experiments, different compressive stress evolutions were observed for different applied overpotentials, and quantitatively associated to the incorporation of hydrogen into the thin film electrode. The higher the cathodic overpotential, the steeper the initial slope of the stress curve, and the faster the stress curves stabilize. From these results, we concluded that the hydrogen absorption rate increases with overpotential, and that the Ni electrode surface saturates faster with adsorbed hydrogen. The amount of hydrogen absorbed into the film was also obtained from these measurements, and compared to the theoretical amount of hydrogen produced by HER calculated from Faraday's law. It was shown that the relative fraction of absorbed hydrogen increases when the applied potential becomes smaller. This was attributed to the fact that the Tafel recombination reaction is slower at low potential, so that hydrogen adatoms still have sufficient time to diffuse into the Ni film. Finally, on the basis of the above observations, we have described the different kinetic regimes that can occur during a polarisation curve as a result of such pronounced Ni-hydride formation.

Acknowledgements

The authors gratefully acknowledge financial support of the Public Service of Wallonia – Department of Energy and Sustainable Building, through the project WallonHY. We also like to cordially thank Ronny Santoro for carrying out the ICP-OES measurements, and Gunnar Lumbeeck and Hosni Idrissi for detailed cross-sectional TEM/ACOM.

References

[1] K.T. Moller, T.R. Jensen, E. Akiba, H. Li, Hydrogen – a sustainable energy carrier, Prog. Nat. Sci.: Materials International 27 (2017) 34–40.
[2] L.M. Gandia, R. Oroz, A. Ursua, P. Sanchis, P.M. Dieguez, Renewable hydrogen production: performance of an alkaline water electrolyzer working under emulated wind conditions, Energy Fuels 21 (2007) 1699–1706.
[3] K. Zeng, D. Zhang, Recent progress in alkaline water electrolysis for hydrogen

production and applications, Prog. Energy Combust. Sci. 36 (2010) 307–326.
[4] A.B. Laursen, A.S. Varela, F. Dionigi, H. Fanchiu, C. Miller, O.L. Trinhammer, J. Rossmeis, S. Dah, Electrochemical hydrogen evolution: sabtier's principle and the Volcano plot, J. Chem. Educ. 89 (2012) 1595–1599.
[5] C. McCrory, S. Jung, I. Ferrer, S. Chatman, J. Peters, T. Jaramillo, Benchmarking hydrogen evolving reaction and oxygen evolving reaction electrocatalysts for solar water splitting devices, J. Am. Chem. Soc. 137 (2015) 4347.
[6] J. Mohammed-Ibrahim, S. Xiaoming, Recent progress on earth-abundant electrocatalysts for hydrogen evolution reaction (HER) in alkaline medium to achieve efficient water splitting – a review, Journal of Energy Chemistry 34 (2019) 111–160.
[7] X. Yao, L. Chen, M. Liu, D. Feng, C. Wang, F. Lu, W. Wang, X. Wang, Y. Cheng, H. Liu, H. Chen, W. Wang, Rational design of Si/TiO_2 heterojunction photocatalysts: transfer matrix method, Appl. Catal. B Environ. 221 (2018) 70–76.
[8] S. Medway, C. Lucas, A. Kowal, R. Nichols, D. Jonhson, In situ studies of the oxidation of nickel electrodes in alkaline solution, J. Electroanal. Chem. 587 (2006) 172–181.
[9] B. McDougall, M. Cohen, Anodic oxidation of nickel in neutral sulfate solution, J. Electrochem. Soc. 121 (1974) 1152–1159.
[10] D.S. Hall, C. Bock, B.R. MacDougall, The electrochemistry of metallic nickel: oxides, hydroxides, hydrides and alkaline hydrogen evolution, J. Electrochem. Soc. 160 (2013) F235–F243.
[11] C.G. Granqvist, E. Avendano, Electrochromic device technology based on nanoporous nanocrystalline thin films on pet foil, The International Society for Optical Engineering 6800 (2007), 680002-1.
[12] F. Blaffart, Q. Van Overmeere, T. Pardoen, J. Proost, In situ monitoring of electrostriction in anodic and thermal silicon dioxide thin films, J. Solid State Electrochem. 17 (2013) 1945–1954.
[13] Chemical Book, Potassium hydroxide, consulted on www.chemicalbook.com.
[14] Q. Van Overmeere, J.-F. Vanhumbeeck, J. Proost, On the use of a multiple beam optical sensor for in-situ curvature monitoring in liquids, Rev. Sci. Instrum. 81 (2010), 045106.
[15] B.E. Conway, J.O.'M. Bockris, R.E. White, Modern Aspects of Electrochemistry, vol. 26, 1994, p. 237.
[16] T. Shinagawa, A.T. Garcia-Esparza, K. Takanabe, Insight on Tafel slopes from a microkinetic analysis of aqueous electrocatalysis for energy conversion, Sci. Rep. 5 (2015).
[17] S.A. Vilekar, I. Fishtik, R. Datta, Kinetics of the hydrogen electrode reaction, J. Electrochem. Soc. 157 (2010) B1040–B1050.
[18] C.H. Hamann, A. Hamnett, W. Vielstich, Electrochemistry, Wiley-VCH, 1998, pp. 167–192.
[19] R. Delmelle, J. Proost, An in-situ study of the hydriding kinetics of Pd thin films, Phys. Chem. Chem. Phys. 13 (2011) 11412–11421.
[20] W.D. Callister, D.G. Rethwisch, Materials Science and Engineering: an Introduction, ninth ed., John Wiley & Sons, 2014.
[21] M. Ruda, D. Farkas, J. Abriata, Embedded-atom interatomic potentials for hydrogen in metals and intermetallic alloys, Phys. Rev. B 54 (1996) 9765–9774.
[22] T.B. Flanagan, F.A. Lewis, Hydrogen absorption by palladium in aqueous solution, Trans. Faraday Soc. 55 (1959) 1400–1408.
[23] Z. Szklarska-Smialowska, Electrical resistance of nickel layers cathodically charged with hydrogen, Bull. Acad. Pol. Sci., Ser. Sci. Chim. 8 (1960) 305–310.
[24] S.S. Srinivasan, D.E. Demirocack, Metal hydrides used for hydrogen storage, in: Y.P. Chen, S. Bashir, J. Liu (Eds.), Nanostructured Materials for Next-Generation Energy Storage and Conversion, Springer, Berlin, Heidelberg, 2017, pp. 225–255.
[25] F.A. Lewis, The hydrides of Palladium and Palladium alloys, Platin. Met. Rev. 4 (1960) 132–137.
[26] Z. Szklarska-Smialowska, M. Smialowski, Creation of stresses in Ni cathodes due to hydrogenation, Bull. Pol. Sci., Ser. Sci. Chim. 6 (1958) 187–193.
[27] D.M. Soares, O. Teschke, I. Torriani, Hydride effect on the kinetics of the hydrogen evolution reaction on nickel cathodes in alkaline media, J. Electrochem. Soc. 139 (1992) 98–105.
[28] S.-M. Kim, S.-H. Jin, Y.-J. Lee, M.H. Lee, Design of nickel electrodes by electrodeposition: effect of internal stress on hydrogen evolution reaction in alkaline solutions, Electrochim. Acta 252 (2017) 67–75.